NMR Implementation of Deutsch-Jozsa and Grover Algorithms

Bhaskar Mookerji and Charles Herder*
MIT Department of Physics
(Dated: March 6, 2008)

We experimentally demonstrate that two-qubit quantum computation using bulk nuclear magnetic resonance (NMR) is possible starting with mixed states at thermal equilibrium. Using a $^{13}CHCl_3$ sample in a Bruker-Avance 200MHz NMR, we emulate pure states through temporal averaging, and subsequently verify the truth tables for a universal controlled-not (CNOT) gate and permutation (SWAP) gate. We also confirm the speedup of quantum algorithms over their classical counterparts by successfully implementing the Deutsch-Jozsa and Grover search algorithms.

Quantum computers use quantum mechanical phenomena, such as superposition and entanglement, for carrying out computation, communication, and data storage, and have been shown to solve certain problems faster than their classical counterparts. A successful implementation requires the mechanism of manipulation *pure* quantum states: creation, unitary transformation, coherent time evolution, and measurement. These requirements pose a practical problem for NMR, where the resulting destructive interference from the statistical mixture of pure states obliterates any necessary coherence.

It turns out that we can fabricate mixed states to contain pure states as subspaces—even at standard room temperature and pressure—which we can use as a basis for computation by a logical labeling of spin quantum number. In the following we will describe how these *effective pure states* can be created in a bulk ensemble NMR at thermal equilibrium. We will also characterize the proper NMR rf pulses and time delays to implement single qubit operations and ultimately universal, two-qubit quantum logic. Using this logic and projective measurement, we will examine two 'fast' quantum algorithms.

1. NMR QUANTUM INFORMATION PROCESSING

We first define a basic unit of quantum computation that is well-characterized and amenable to external perturbation. For our NMR system, the S_z basis of a spin-1/2 particle in a magnetic field describes a state $|\psi\rangle = \alpha\,|+1/2\rangle + \beta\,|-1/2\rangle$. This basis can be labeled as a $|0\rangle$ and $|1\rangle$, respectively, forming a *qubit*. The two-qubit system used in this experiment, carbon-13 labeled chloroform ($^{13}CHCl_3$), is a heteronuclear molecule of two strongly-coupled spin-1/2 particles described by the Hamiltonian

$$H = -\hbar\omega_L^H S_z^H - \hbar\omega_L^C S_z^C + 2\pi\hbar J S_z^H S_z^C, \qquad (1)$$

where spin S_z^H and S_z^C operators (and their resonant frequencies) belong to the ^{1}H and ^{13}C nuclei, respectively, and J is the coupling constant of their nuclear spins. The product eigenstates of this Hamiltonian are $|m_H, m_C\rangle$, where $m_H = \pm 1/2$, $m_C = \pm 1/2$ are the eigenvalues of S^H and S^C, respectively. In order of increasing energy, these eigenstates are defined as our computational basis $\{|00\rangle, |01\rangle, |10\rangle, |11\rangle\}$. This basis is observable, as transitions between these levels are allowed according to the angular momentum selection rules $\Delta m_{H,C} = \pm 1$. Consequently, there are four peaks in the full NMR spectrum at the frequencies $\omega_C \pm \pi J$ and $\omega_H \pm \pi J$, the separation of each doublet given by $2\pi J$.

Acting on this basis, NMR can create a universal set of logic gates through unitary transformations. Note here that *any* arbitrary unitary transformation in a $2-$dimensional Hilbert space can be decomposed as

$$\begin{aligned} U(N) &= U(1) \times SU(N) \\ &\xrightarrow{N=2} e^{i\phi} R_x(\alpha)\, R_y(\beta)\, R_z(\gamma), \end{aligned} \qquad (2)$$

where any arbitrary rotation about a unitary vector $\hat{n}$ with total spin $\mathbf{S}$ is given by $R_{\hat{n}}(\theta) = \exp(-i\theta\hat{n}\cdot\mathbf{S})$, a common rotation transformations in NMR on a spin-1/2 particle using rf pulses with the required phase. Phase transformations are given by free-evolution through spin-spin coupling operator $\tau = \exp[-i(\pi/4)\,\sigma_z \otimes \sigma_z]$. Finally, generalizing to a product space, we can selectively apply unitary transformations at the resonance frequency ω_i of a given nucleus such that $U^H U^C = U \otimes U$.

1.1. Effective Pure States and Temporal Averaging

Our proceeding discussion centered around an ideal spin-1/2 nucleus in a magnetic field. However, in the ensemble picture our sample in thermal equilibrium is represented by the density matrix

$$\rho_{\text{th}} = \frac{e^{-H/k_B T}}{Z} \qquad (3)$$

with canonical partition function $Z = \text{Tr}\, e^{-E_k/k_B T}$. In high temperature limit $k_b T \gg \hbar\omega$ this is given by

$$\begin{aligned} \rho_{\text{th}} &= \text{diag}(a, b, c, d) && (4) \\ &\approx \frac{I}{4} + 10^{-4}\text{diag}(5, 3, -3, -5), && (5) \end{aligned}$$

*Electronic address: mookerji@mit.edu; URL: http://web.mit.edu/8.13/

where diagonal elements specify the probability of a particle being found an element of our ordered basis[1].

Provided that some members of the ensemble are in the desired ground state $|00\rangle$, we can either arrange the remaining states such that their signals cancel or average out, and what remains will behave like a pure basis state. Consider a computation a trace-preserving unitary transform $C(\rho) = \sum_k A_k \rho A_k^\dagger$ such that $\sum_k A_k^\dagger A_k = I$, and a general Hermitian observable written as $\hat{n} \cdot \vec{\sigma}$, where $\vec{\sigma}$ is a vector of Pauli matrices. An effective pure state is a state that can be written to include a pure state:

$$\rho = \frac{1-\alpha}{2^N} I + \alpha |\psi\rangle \langle\psi| . \tag{6}$$

In the ensemble picture , any transformation on this density matrix is equivalent to carrying out that transformation on the pure state itself, as

$$\mathrm{Tr}\left[C(\rho)(\hat{n}\cdot\vec{\sigma})\right] = \alpha \mathrm{Tr}\left[C(|\psi\rangle\langle\psi|)(\hat{n}\cdot\vec{\sigma})\right] . \tag{7}$$

From Equation 7, it is sufficient to simulate the ground state by the process of temporal averaging, such that adding to the thermal state permutations of itself, an effective ground state is formed,

$$U(\rho_{\mathrm{th}} + \rho_2 + \rho_3) U^\dagger = (1-a) I + (4a-1) U(|00\rangle\langle 00|) U^\dagger . \tag{8}$$

This permutation transformation is carried out by the controlled-NOT (CNOT) gates, which can act to take $|HC\rangle$ to either $|H, H \oplus C\rangle$ ('A') or $|H \oplus C, H\rangle$ ('B'). The truth table of the first is given by

$$\begin{aligned} U_{\mathrm{CN}}^A &= \begin{bmatrix} 1 & 0 & 0 & 0 \\ 0 & 1 & 0 & 0 \\ 0 & 0 & 0 & 1 \\ 0 & 0 & 1 & 0 \end{bmatrix} \\ &= e^{-i\pi/4} R_y^A \tau \bar{R}_y^A \bar{R}_x^A \bar{R}_x^B R_y^B R_x^B \end{aligned} \tag{9}$$

where the second line gives the unitary transformation as a product of $\pm\pi/2$ rf pulses and an overall irrelevant phase factor. Letting $U_1 = U_{\mathrm{CN}}^B U_{\mathrm{CN}}^A$ and $U_2 = U_1^\dagger$, the effective ground state $|00\rangle$ is created with $\rho_1 = U_1 \rho_{\mathrm{th}} U_1^\dagger$ and $\rho_2 = U_2 \rho_{\mathrm{th}} U_2^\dagger$[2].

2. EXPERIMENTAL SETUP AND PROCEDURE

A block diagram of our experiment is in Figure 1. Bruker-Avance 200MHz NMR applied RF pulses to the nuclear spins of ^{13}C and ^{1}H atoms in a 7% solution of chloroform ($^{13}CHCl_3$) dissolved in d_6-acetone, degassed, and flame-sealed in a 5mm glass tube at room temperature and standard pressure. Any given pulse experiment begins with a delay period during with longitudinal relaxation allows the nuclei to return to their thermal equilibrium state. Transverse rf pulses apply selective rotations of spin at the resonance frequencies of individual

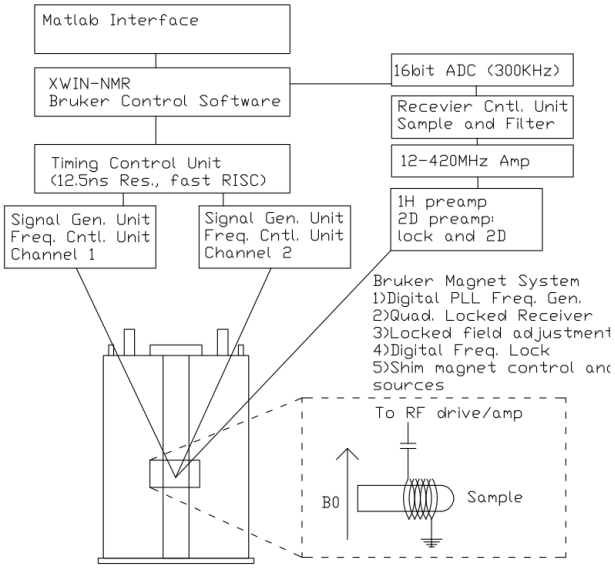

FIG. 1: Block diagram of the liquid-state NMR apparatus used to implement a two-qubit quantum computer. A superconducting magnetic provides a static, homogeneous magnetic field at 4.7T and is shimmed by secondary Helmholtz coils to provide homogeneity to $10^{-9}/\mathrm{cm}^3$. The sample is spun to average out further inhomogeneities in the axial field. Transverse coils transmit and receive rf pulses in a phase-locked loop (PLL) using the d_6-acetone signal as a frequency reference.

atoms. We measure a proton or carbon state by applying an R_x pulse to the required qubit. The resulting free induction decays are Fourier transformed to a spectrum whose peaks are attributed to the spin states in Section 1. Pulse sequences were controlled through a Matlab interface to the xnmr control program with which we specified pulse widths (for $\pi/2$), phases ($\pm x$ $\pm y$), free-rotation delay time ($\tau = 1/2J$), and initial state (thermal state or ground state through temporal averaging.).

Before applying our pulse procedure, we measure the required parameters necessary for applying unitary transformations and performing measurement on a coherent time scale. First, we determine the time scale of decoherence of our quantum computer through a $2\pi - \Delta t - \pi$; the time scale of decoherence through spin-lattice interactions is given by $T_1 = 17.0 \pm 0.5$s ($\chi^2 = 0.85$). The decay scale of spin-spin interactions is given by the line width of a spectral peak $2/T_2$ and was determined to be $T_2 = 2.04 \pm 0.09$ ($\chi^2 = 1.521$). For fidelity of unitary transformations, we integrated the spectral peaks for a series of pulse times for ^{1}H and ^{13}C channels. The pulse width of ^{1}H and ^{13}C are determined to be 9.3 ± 0.3ms ($\chi^2 = 1.4$) and 7.8 ± 0.1ms ($\chi^2 = 1.02$), respectively. Through a double Lorentzian fitting, the spin-spin coupling constant for phase delay is given by $J = 215.05 \pm 0.02$Hz ($\chi^2_{\mathrm{Right}} = 1.5$ and $\chi^2_{\mathrm{Right}} = 0.84$). To keep the imaginary component of a given spectrum to $< 10\%$ the real part, phase angles are corrected in

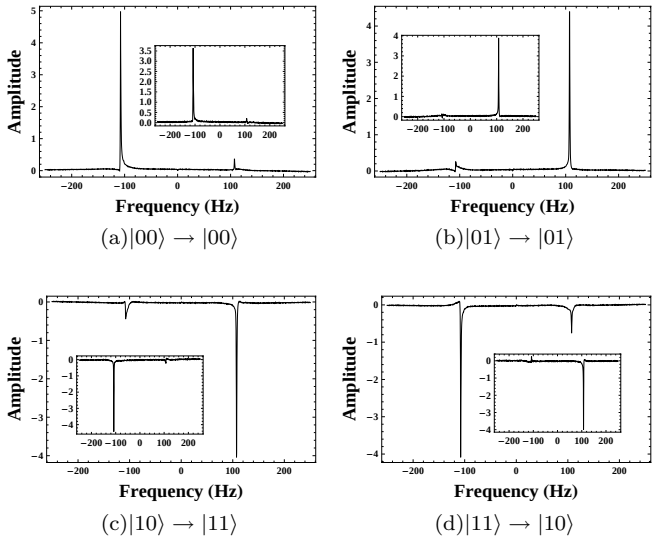

FIG. 2: Proton NMR truth table for U_{CN}. The inset spectrum indicates the initial basis state of the transformation.

software through calibration, and a time delay of 50s between iterations of temporal averaging allows the system to return to thermal equilibrium.

3. RESULTS AND ERROR ANALYSIS

In the following we discuss our pulse sequence implementation and results for a CNOT gate, a SWAP gate using a series of CNOT gates, and two non-trivial quantum algorithms: the Deutsch-Jozsa and Grover search algorithms. For the CNOT and SWAP gates we reconstruct the diagonal elements of the density matrices for the final states. If a given density matrix were written as the first matrix term in Equation 5, then the real values of the peak integrals of the first qubit (^{1}H) correspond to $a-c$ and $b-d$. The peaks for the second qubit (^{13}C) are given by $a-b$ and $c-d$. This density matrix being traceless, we can then solve for the values of a, b, c, and d using linear least-squares method. The relative error in the density matrices is given by

$$\sigma_\rho = \frac{||\rho^{\mathrm{Exp.}} - \rho^{\mathrm{Theory}}||}{||\rho^{\mathrm{Theory}}||}. \tag{10}$$

Typically, error on individual elements of density matrices ranged between 2% and 26%, with cumulative error between 24% and 80%.

3.1. Two-Qubit Quantum Logic: CNOT and SWAP

Using temporal averaging on the thermal state of our sample, we measured the truth table for the CNOT gate on our labeled basis, which is found in Equation 9. Reconstructed density matrices for the CNOT gate on the labeled basis and the thermal states are given in Figure 6. Note that the $|00\rangle$ and $|10\rangle$ states are left unchanged, while the latter two states have had their lower bits inverted.

We have reconstructed the diagonal elements of CNOT gate on the thermal state and the pure states. Disregarding an overall 10^4 scale factor, the measured thermal state density matrix after a CNOT gate is

$$U^A_{\mathrm{CNOT}}\rho_{\mathrm{Thermal}}U^{A\dagger}_{\mathrm{CNOT}} = \begin{bmatrix} 351. & 0 & 0 & 0 \\ 0 & 232. & 0 & 0 \\ 0 & 0 & -350. & 0 \\ 0 & 0 & 0 & -233. \end{bmatrix}, \tag{11}$$

where each element of the density matrix has associated with it an integration error of ± 43, yielding a peak ratio of 1.51 ± 0.11 within 2σ of the expected $5/3 \approx 1.67$. The expected behavior of the thermal state is left invariant under the action of a CNOT, and so the theoretical value of density matrix is given by the second term of Equation 5.

We can also extend the CNOT gate into a gate that swaps the states of two qubits. Extending the permutation operation mentioned briefly in Section 1.1, the series of operations to flip the qubits are given by

$$\begin{aligned} |H, C\rangle &\xrightarrow{\mathrm{CN}^A} |H, H \oplus C\rangle \\ &\xrightarrow{\mathrm{CN}^B} |H \oplus (H \oplus C), H \oplus C\rangle = |C, H \oplus C\rangle \\ &\xrightarrow{\mathrm{CN}^A} |C, (H \oplus C) \oplus C\rangle = |C, H\rangle . \end{aligned} \tag{12}$$

Accordingly, the spectra from this gate on our basis is given in Figure 5. Here, the SWAP transformation leaves unchanged the $|00\rangle$ and $|11\rangle$ states, but flips the $|01\rangle$ and $|10\rangle$[2].

3.2. Deutsch-Jozsa Algorithm

In addition to two-qubit quantum logic, we also implemented a two-qubit simple version of the Deutsch-Jozsa algorithm. This algorithm determines if a function $f(x)$ acting on N bits returns exactly $f(x) = 0$ for all x, or exactly $f(x) = 1$ for all x (called *constant*); or returns exactly $f(x) = 0$ for half the inputs and $f(x) = 1$ for the rest (called *balanced*). Determining with certainty whether a function is constant or balanced on a deterministic classical computer has order of growth $O\left(2^{N-1} - 1\right)$. A quantum computer exploits superposition states to evaluate all function possibilities at once.

A quantum circuit diagram, pulse sequence, and truth table depicting the Deutsch-Jozsa algorithm for a unitary transformation U_f acting on the vacuum state $|00\rangle$

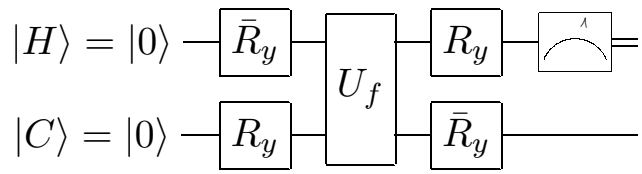

	Constant functions		Balanced functions	
	Case 1	Case 2	Case 3	Case 4
$f(0)$	0	1	0	1
$f(1)$	0	1	1	0
$w \oplus f(a)$	ID	NOT	CNOT	Z-CNOT

FIG. 3: A quantum circuit of the Deutsch-Jozsa algorithm exhibits "quantum parallelism." (top) The target and the control qubits are rotated into the superposition states $(|0\rangle \pm |1\rangle)/\sqrt{2}$ and then evaluated by U_f. The control qubit now contains the outputs of f on all possible inputs. (bottom) Truth table and pulse sequences for functions f_1 through f_4.

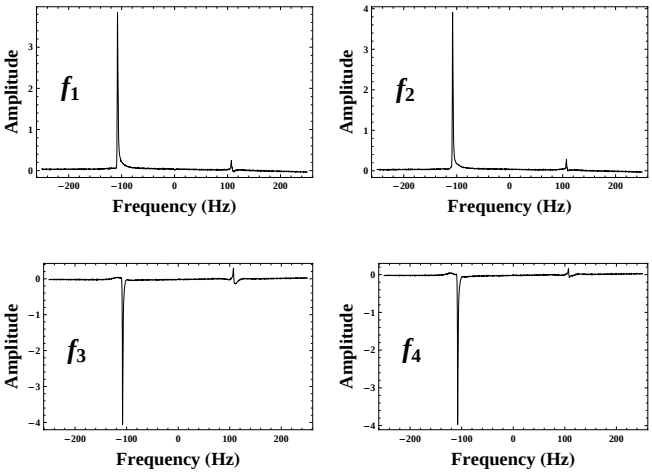

FIG. 4: Proton NMR truth table for the Deutsch-Jozsa algorithm. Functions f_1 and f_2 are constant, while functions f_3 and f_4 are balanced.

is shown in Figure 3[1]. The ground state is rotated into a maximally mixed state and evaluated by the function through a unitary transformation. At this point, the function has been evaluated for all possible values:

$$\frac{1}{2}\left((-1)^{f_k(0)} + (-1)^{f_k(1)}\right)|00\rangle + \frac{1}{2}\left((-1)^{f_k(0)} - (-1)^{f_k(1)}\right)|10\rangle \quad (13)$$

Applying the reverse transformation, the state collapses into $|f_k(0) \oplus f_k(1), 0\rangle$, where $f_k(0) \oplus f_k(1) = 0$ if f_k is constant and $f_k(0) \oplus f_k(1) = 1$ is balanced. The resulting spectra from the NMR implementation is given in Figure 4.

3.3. Grover Search Algorithm

Our remaining algorithm solves the problem of identifying an element in an unordered database of size N in $O\left(\sqrt{N}\right)$ evaluations, as opposed to $O(N)$ evaluations for a classical computer. A black box *oracle* O behaves as the identity except for the *winner*, whose phase is inverted. The oracle transformation is passed a maximally mixed state through a rotation transformation $H^{\otimes 2}$ and is then rotated by a phase by operator P. The algorithm rotates an angle dependent on the number of bits in the search string until the winner is found. The algorithm continues to rotate after finding the winner and oscillates between the winner and the initial state[2].

We executed Grover's algorithm for a long and short set of pulses. Defining the aforementioned matrices with the rotations,

$$\begin{aligned} O &= R_y^C R_x^C \bar{R}_y^C R_y^H R_x^H \bar{R}_y^H \tau \\ P &= R_y^C \bar{R}_x^C \bar{R}_y^C R_y^H \bar{R}_x^H \bar{R}_y^H \tau \\ H^{\otimes 2} &= R_x^C R_x^C R_y^C R_x^H R_x^H R_y^H \end{aligned} \quad (14)$$

the Grover algorithm operator is given by

$$G = H^{\otimes 2} P H^{\otimes 2} O, \quad (15)$$

which finds the winner when applied to the ground state,

$$|\psi_G\rangle = G^n H^{\otimes 2} |00\rangle . \quad (16)$$

Removing redundant rotations, our shorter pulse sequence is given by,

$$G = \bar{R}_x^C \bar{R}_y^H \bar{R}_x^H \bar{R}_y^H \tau \bar{R}_x^C \bar{R}_y^H \bar{R}_x^H \bar{R}_y^H . \quad (17)$$

We observed that the shorter pulse sequence found the winning element in the theoretically predicted $n = 4$ iterations, while the longer sequence found the winner in $n = 5$ iterations. This suggested that accumulated error from $\pi/2$ pulses contributed to error in the longer pulse sequence. A simulated pulse sequence of Grover's algorithm accounting for artificial errors in our pulse sequences with an offset -0.01μs (^{1}H) and 0.02μs (^{13}C) reproduced the periodic behavior qualitatively, oscillating between the maximally mixed state and the winner $|11\rangle$.

3.4. Error Analysis

Several factors contribute to systematic and statistical error in our experiment. The experiment was automated

[1] Figure taken from S. Gulde, "Implementation of the DeutschJozsa algorithm on an ion-trap quantum computer" Nature 421, 48-50 (2 January 2003)

in hardware and software, limiting our sources of statistical error to phase drift and negligible white noise. A low signal-to-noise ratio for carbon spectra required larger data sets for accurate pulse width measurement. The most relevant systematic error was the precision and accuracy of $\pi/2$ pulse widths. Error from this effect is cumulative and is measurable in multiple iterations of long algorithms, such as the Grover search algorithm. Asymmetric Lorentzian line shapes likely resulted from inhomogeneities stemming from suboptimal shimming, as well as imaginary components from imperfect phase of our peaks. In this case, it's worth pointing out that our resonance frequency selective pulses do not completely suppress spin-spin (J) couplings during a pulse sequence, thereby introducing some out of phase imaginary component. Further cumulative error is from incomplete relaxation to thermal equilibrium during experiments is also cumulative.

Some of these factors contribute to our density matrix characterization, another significant component is the trapezoidal integration algorithm used in the experiments MATLAB control scripts. This is problematic, particularly for groups relying on immediate feedback from the control software by using real and complex peak integrals and phase correction. Our measured diagonal elements of the density matrices could be significantly improved with a higher-order numerical integration method, such as Simpson's rule.

3.5. Conclusion

In summary, we have discussed the input-state preparation problem for liquid state NMR, its solution through temporal averaging, and the relevant experimental parameters for maintaining a NMR quantum computer on a coherent time scale. Universal quantum logic and algorithms implemented through it are possible, but spectacularly difficult (if not theoretically impossible) to scale to significantly higher numbers of qubits.

Acknowledgments

B. Mookerji thanks C. Herder for his equal contribution to the this experiment and its analysis, and the Junior Lab staff.

[1] N. A. Gershenfeld and I. L. Chuang, SCIENCE: Science **275** (1997), URL citeseer.ist.psu.edu/gershenfeld97bulk.html.

[2] E. A. J. C. C. F. Ivan Oliveira, Tito Bonagamba, *NMR Quantum Information Processing* (Elsevier, 2007).

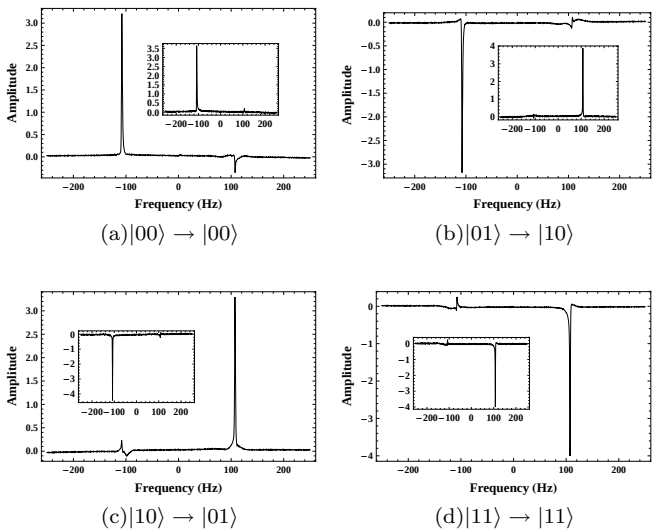

(a)$|00\rangle \rightarrow |00\rangle$ (b)$|01\rangle \rightarrow |10\rangle$

(c)$|10\rangle \rightarrow |01\rangle$ (d)$|11\rangle \rightarrow |11\rangle$

FIG. 5: Proton NMR truth table for U_{SWAP}. The inset spectrum indicates the initial basis state of the transformation.

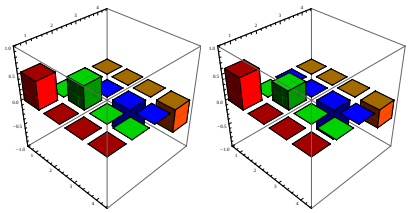

(a)Thermal (Measured)$_{40.0\%}$ (b)Thermal (Theoretical)

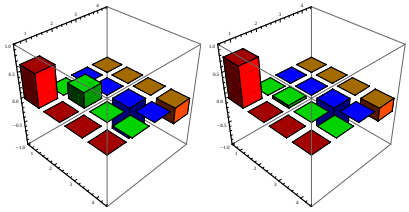

(c)$|00\rangle \rightarrow |00\rangle_{61.1\%}$ (d)$|00\rangle$

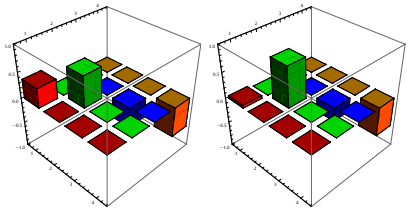

(e)$|01\rangle \rightarrow |01\rangle_{54.4\%}$ (f)$|01\rangle$

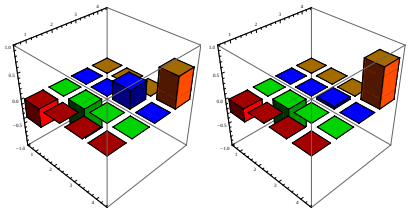

(g)$|10\rangle \rightarrow |11\rangle_{79.1\%}$ (h)$|11\rangle$

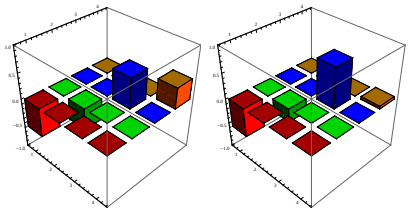

(i)$|11\rangle \rightarrow |10\rangle_{71.1\%}$ (j)$|11\rangle$

FIG. 6: Experimentally measured deviation density matrices for CNOT truth table on the thermal state and a two-qubit computational basis (normalized to ± 1). Assuming that off-diagonal coherences are 0, results for the basis stats and the thermal state qualitatively match expectations for the CNOT truth table described by Equation 9. Relative errors for the entire state is given by $||\rho^{\text{Exp.}} - \rho^{\text{Theory}}||/||\rho^{\text{Theory}}||$. Relative errors for the diagonal elements ranged between 1 and 22%.